



## Heavy metals adsorption onto graphene oxide: effect of mixed systems and response surface methodology modeling

Ahmed Ibrahim<sup>a</sup>, Muhammad S. Vohra<sup>a,b,\*</sup>, Salem A. Bahadi<sup>c</sup>, Sagheer A. Onaizi<sup>c,d</sup>, Mohammed H. Essa<sup>a</sup>, Tariq Mohammed<sup>a</sup>

<sup>a</sup>*Civil and Environmental Engineering Department, King Fahd University of Petroleum and Minerals (KFUPM), Dhahran 31261, Saudi Arabia, Tel. +966-013-860-2854; emails: vohra@kfupm.edu.sa (M.S. Vohra), g201704750@kfupm.edu.sa (A. Ibrahim), mhessa@kfupm.edu.sa (M.H. Essa), mktariq@kfupm.edu.sa (T. Mohammed)*

<sup>b</sup>*Interdisciplinary Research Center for Construction and Building Materials, King Fahd University of Petroleum and Minerals (KFUPM), Dhahran 31261, Saudi Arabia*

<sup>c</sup>*Chemical Engineering Department, King Fahd University of Petroleum and Minerals (KFUPM), Dhahran 31261, Saudi Arabia, email: g201473540@kfupm.edu.sa (S.A. Bahadi), onaizi@kfupm.edu.sa (S.A. Onaizi)*

<sup>d</sup>*Interdisciplinary Research Center for Hydrogen and Energy Storage, King Fahd University of Petroleum and Minerals (KFUPM), Dhahran 31261, Saudi Arabia*

Received 16 October 2021; Accepted 1 June 2022

---

### ABSTRACT

Competitive adsorption based removal of aqueous cadmium, chromium, and lead from tertiary mixed systems, was investigated using graphene oxide (GO). The surface characterization findings indicated that the produced GO is mesoporous with several oxygen based functional groups important for the adsorption of target heavy metal species. Under the respective tertiary competitive adsorption conditions, a near complete chromium removal was noted (~99%) at GO dosage of 0.5 g/L. Similarly the adsorption capacity of lead was also high at ~92% at a GO dosage of 0.5 g/L. Nevertheless, the cadmium showed a lower removal of ~51% under the competitive conditions. In general, the competitive removal of these heavy metals showed the following trend: chromium > lead > cadmium. These findings show that the synthesized graphene oxide preferentially adsorbs chromium and lead compared to cadmium. The oxygen surface functional groups, as indicated by the Fourier transform infrared spectroscopy analysis, are suggested to initiate the metal bonding and adsorption. Furthermore, the Brunauer–Emmett–Teller characterization results showed that the synthesized GO is mesoporous that is also supportive of an enhanced mass transfer to the surface bonding sites. The respective response surface methodology based process modeling and optimization also yielded good outcomes, for example, for lead removal, the respective analysis of variance findings showed that the GO dosage and concentration of lead and chromium are the significant model parameters with respective *F*-values of 267.48, 52.27, and 12.09, and respective *p*-values of <0.0001, <0.0001, and 0.0031. Furthermore, both the normal probability plot and the predicted vs. actual response plot also showed a good fit for the studied metal adsorption on to synthesized graphene oxide.

*Keywords:* Graphene oxide; Adsorption; Cadmium; Chromium; Lead

---

\* Corresponding author.

## 1. Introduction

Heavy metal pollution and specifically mixed heavy metals environmental contamination of fresh water sources remains a concern in several regions across the globe. For example cadmium related aquatic contamination is reported at various National Priority List (NPL) sites of U.S. EPA [1,2]. Cadmium is also released into environment from several industries and landfill sites [3] and poses several health issues including cancer and damage to kidney [4]. Furthermore, lead is another toxic metal that is also introduced into environment via anthropogenic activities like mining, fossil fuel combustion, and specific industrial setups [5–8]. Lead can also initiate damage to human organs including brain and kidney [9,10], and therefore lead related water environmental standards are very stringent [11,12]. Furthermore, chromium is another toxic heavy metal species with concerns such as damage to respiratory tract. It is introduced into environment from sources including metallurgical operations, tanning practices, and paint and fertilizers manufacturing [13,14], with Cr(VI) being more toxic as compared to Cr(III) [15,16]. Hence, the respective cadmium, chromium, and lead toxicity concerns require an appropriate treatment of such contaminated water bodies.

Various treatment methods have been reported for the removal of toxic metal species from the aqueous phase. These technologies include electro-coagulation, adsorption, photocatalysis, membrane systems, and precipitation [17–22]. For example layered double hydroxide based exchangers, have been reported to treat aquatic lead and chromium [9,14]. Similarly physical systems such as membrane filtration and chemical redox processes including electro-coagulation and photocatalysis have also been employed for the same. Furthermore, several adsorption based applications are also reported including cadmium and lead removal using carbon nanotubes [4,7], lead removal using activated carbon produced from organic wastes [5,6,8,], natural biosorbents [10], resin material [12], and chromium removal using biosorbent [16]. The respective adsorption systems offer several advantages including the usage of production of adsorbents from agricultural wastes and no sludge or concentrate remaining as is the case for precipitation or membrane systems.

The above discussion highlights the need for toxic metals from the aqueous phase, along with the technologies in use. However one important concern is the presence of metals in a mixed state and resulting synergistic competition poses a challenge. This requires investigating other treatment methodologies. To that end, the mesoporous graphene oxide (GO); which is a 2D nanomaterial with a hexagonal lattice structure of pure carbon atoms) has received much attention for environmental cleanup. Mesoporous GO can be synthesized via the chemical oxidation of natural graphite, also known as graphite oxide sheet [23]. The respective sheets are rich in oxygen and carry hydroxyl and epoxide functional groups in interplanar spacing and carboxyl and carbonyl functional groups located on sheet edges. Because of such functional groups, GO is considered to be a promising adsorbent in the area of aqueous heavy metals and radionuclides removal [24–27]. The functional groups' oxygen has lone electron pair that can interact with metal ions and form metal complexes [28]. Furthermore, the inter-planar spacing is higher in the

synthesized GO as compared to the parent graphite, which also helps to yield a greater interaction with the heavy metal species [29]. Considering this graphene, graphene oxide, and modified graphene oxide materials have been used to remove heavy metals from water [30,31], including cadmium [32–34], lead [35–39], and chromium [36,37,40] and also some binary systems [41–43]. Chromium because of its respective toxicity concerns has also been treated using GO/modified-GO along with process optimization exercise [44–46]. Furthermore, GO modified membranes systems have also been used for heavy metals removal [47,48]. Nevertheless, the removal of respective toxic metal species from the aqueous phase using graphene oxide will also need to consider the competitive removal trends under a varying set of conditions including tertiary systems. Thus the present work explored several matrices of cadmium, chromium and lead under changing aqueous phase settings that to the best of our knowledge, has not been investigated. The outcomes include both the surface characterization of produced GO material and its adsorption efficiency determination. Furthermore the surface response surface methodology (RSM) based statistical modeling that has been successfully reported for the optimization adsorption process, was also employed for the present work [49,50]. The respective findings are promising, and details are reported in sections below.

## 2. Materials and methods

### 2.1. Materials

The reagent grade high purity chemicals used in the present work included pure graphite powder (Fisher, USA), phosphoric acid ( $H_3PO_4$ , 85% w/w, Baker, UK), sulfuric acid ( $H_2SO_4$ , 97% w/w, Fisher, USA), hydrochloric acid (HCl, Fisher, USA), potassium permanganate ( $KMnO_4$ , Fisher, USA), 30% hydrogen peroxide ( $H_2O_2$ , Baker, UK), cadmium nitrate tetrahydrate ( $Cd(NO_3)_2 \cdot 4H_2O$ ), Fisher, USA), lead nitrate ( $Pb(NO_3)_2$ , Fisher, USA), chromium chloride hexahydrate ( $CrCl_3 \cdot 6H_2O$ , Fisher, USA), and sodium hydroxide (NaOH, Fisher, USA).

### 2.2. Synthesis of graphene oxide

The improved Hummers Method was used to synthesize the graphene oxide (GO) in our lab as also shown in the Fig. 1 [51]. In a typical synthesis technique, a 1 L flask was first filled with 360 mL concentrated sulfuric acid (97%) and 40 mL concentrated phosphoric acid (85%) that was stored in an ice bath. While continuously mixing, 3 g of graphite powder was added to that acidic mixture followed by a gradual 18 g  $KMnO_4$  addition (mass ratio of graphite: $KMnO_4$  = 1:6). Once the  $KMnO_4$  addition was complete, the flask was removed from the ice bath and placed in a water bath. The water bath was heated to 50°C and held there for 12 h. The solution was then cooled to room temperature before being poured into a ~400 g crushed ice bag (prepared using distilled water). After stirring for 10 min, 6 mL of 30%  $H_2O_2$  was added to the resulting material. The generated GO was then separated by centrifugation at 4,000 rpm for 15 min. Subsequently, the separated GO was washed multiple

times with distilled water and 10% HCl, and then rinsed again with distilled water before being dried at 50°C until completely dry (approx. 2–3 d).

### 2.3. Characterization of graphene oxide

The X-ray diffraction (XRD) analyses of synthesized graphene oxide was first completed using Cu K radiation in the 2 range of 0°–70° at 40 kV and 30 mA. Scanning electron microscopy (SEM) technique was also used to characterize the surface morphology of the produced GO at 20 kV and 30,000 magnification whereas the elemental composition of GO was measured using the energy-dispersive X-ray spectroscopy (EDX) technique. Prior to SEM and EDX measurement, the GO sample was coated with 10 nm gold. Furthermore, the surface functional groups were identified using the Fourier transform infrared spectroscopy (FTIR) technique in range of 400–4,000 cm<sup>-1</sup>. The specific surface area, pore-volume, and pore size were obtained using N<sub>2</sub> adsorption/desorption isotherms at 77 K with relative pressures (p/p°) ranging from 0 to 1 along with the respective Brunauer–Emmett–Teller (BET) adsorption modeling software (Micromeritics, U.S.A.).

### 2.4. Adsorption study

The cadmium, chromium, and lead stock solutions (1,000 mg/L) were first prepared and then used for respective metals-GO adsorption experiments. The adsorption experiments were completed at adsorbent dosages of 0.2, 0.35, and 0.5 g/L and metal concentrations of 5, 7.5, and 10 mg/L. For all adsorption experiments, initially a 250 mL of mixed solution was prepared, out of which a 50 mL sample was collected as the blank and the remaining 200 mL solution was used for the adsorption experiment. The pH was always adjusted to 4 with continuous complete mixing for 24 h (at room temperature) followed by sample collection and filtration (0.2 μ membrane filter; Whatman, Germany). The respective samples were analyzed for cadmium, chromium and lead using the atomic absorption spectroscopy (Perkin Elmer, U.S.A.) and the respective metal removal percentage was calculated using Eq. (1):

$$\% \text{Metal Removal} = \frac{C_0 - C_e}{C_0} \times 100 \quad (1)$$

C<sub>0</sub> = initial metal concentration; C<sub>e</sub> = metal concentration at equilibrium

### 2.5. Response surface methodology

Response surface methodology (RSM) is a statistical approach that is used to design, improve, and optimize processes under a varying set of operational variables. It is employed when several variables could have an impact on a process' performance. The response is represented by the performance measure, and the factors are independent variables. For the present work, the adsorbent dosage and cadmium/chromium/lead concentration were the independent variables. The respective values for the 'range of variables' is provided in Table 1. The Design-Expert software was used for the present RSM work. Furthermore,

the central composite design (CCD) with four factors and a single center point of face-centered (FCC) as illustrated in Table 1 was used to create design of experiment as shown in Table 2 [52].

## 3. Results and discussion

### 3.1. Graphene oxide characterization details

Though the pristine graphite exhibits an intense XRD peak at a 2θ ~26° [53,54], however when graphite is oxidized to GO using the improved Hummers Method, the XRD pattern shifts to 10°, as noted in Fig. 2. The diffraction peak at 2θ ~10° corresponds to the crystallographic plane indexed as (002) in the hexagonal structure of GO [54]. When pristine graphite is oxidized to GO, a large number of oxygen-containing functional groups such as hydroxyl, epoxy, and carboxyl are attached to the carbon atoms, causing the diffraction peak to shift to a lower angle. The intercalation of the oxygen-containing functional groups into graphite results in the expansion of the interplanar spacing from about 0.34 nm in the pristine graphite [53,55] to about 0.93 nm in the obtained GO. The XRD pattern shown in Fig. 2 also displays a small diffraction peak at a 2θ angle of ~43°, which might be attributed to a short-range order in the stacked GO layers [56].

The morphology of GO was also investigated using SEM technique. As shown in Fig. 3a, GO has a lamellar structure that is composed of flakes and folded graphitic sheets due to the oxidation of graphite, leading to the attachment of

Table 1  
Levels of main factors as employed for the RSM modeling

Factor	-1 (Low)	0	+1 (High)
GO (g/L)	0.2	0.35	0.5
Cd (mg/L)	5	7.5	10
Cr (mg/L)	5	7.5	10
Pb (mg/L)	5	7.5	10

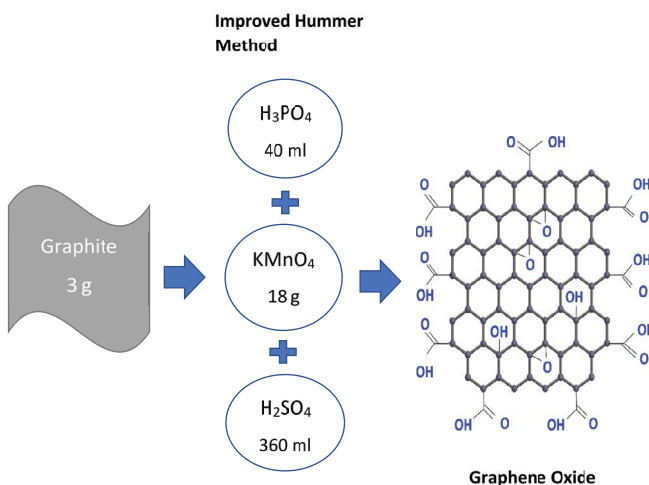


Fig. 1. General process for graphene oxide synthesis using the improved Hummer method.

Table 2  
RSM design of adsorption experiments

Run	Factor 1	Factor 2	Factor 3	Factor 4	RE. Cd	RE. Cr	RE. Pb
	A:Dose	B:Cd	C:Cr	D:Pb			
	g/L	mg/L	mg/L	mg/L			
1	0.5	5	5	5	50.57	97.33	91.77
2	0.35	7.5	7.5	5	49.33	93.49	90.84
3	0.2	7.5	7.5	7.5	5.75	78.86	46.83
4	0.2	5	10	10	7.60	62.44	46.86
5	0.2	5	5	10	10.29	77.57	65.18
6	0.2	5	10	5	7.98	60.15	56.51
7	0.35	7.5	7.5	10	16.40	78.40	73.33
8	0.2	10	5	10	10.62	81.00	67.45
9	0.35	5	7.5	7.5	15.40	83.07	75.24
10	0.5	5	5	10	39.92	97.52	89.51
11	0.5	5	10	10	17.00	83.14	79.00
12	0.35	10	7.5	7.5	14.75	85.40	77.98
13	0.35	7.5	7.5	7.5	16.83	86.87	80.66
14	0.5	10	5	5	43.86	98.76	90.64
15	0.35	7.5	10	7.5	11.48	78.21	69.95
16	0.2	10	10	5	5.20	60.78	49.32
17	0.5	5	10	5	25.00	89.37	85.40
18	0.5	10	10	10	14.93	87.17	77.39
19	0.5	10	5	10	31.60	89.75	86.94
20	0.5	10	10	5	22.58	87.75	83.58
21	0.2	10	5	5	10.80	75.00	64.81
22	0.5	7.5	7.5	7.5	26.02	93.07	83.72
23	0.2	5	5	5	10.00	86.64	64.17
24	0.2	10	10	10	5.26	65.40	33.19
25	0.35	7.5	5	7.5	22.75	88.09	81.70

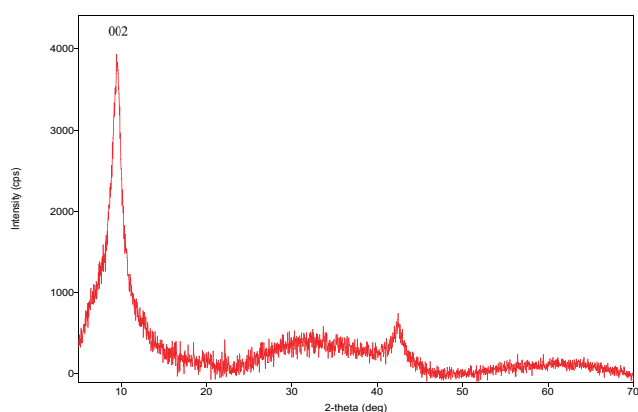


Fig. 2. XRD pattern of synthesized graphene oxide.

oxygen-containing functional groups to the graphitic sheets [57,58]. Fig. 3b shows the elemental composition of GO. The synthesized GO contains about 60.8 and 39.2 w/w% carbon and oxygen, respectively, corresponding to a C/O atomic ratio of 2.07, which is in line with the proposed typical C/O

atomic ratio (i.e., 2.0–3.0) of graphene oxide [59–61]. Fig. 4 shows the FTIR spectra of GO in the wavenumber range 400–4,000  $\text{cm}^{-1}$ . The % transmittance spectra shows an intense and broad peak centered at 3,400  $\text{cm}^{-1}$ , which represents the O–H stretching vibration while the minor peaks at around 2,920 and 2,850  $\text{cm}^{-1}$  correspond to the C–H bending vibration [62,63]. Additionally, the peak appearing at 1,750  $\text{cm}^{-1}$  is associated with the C=O stretching vibration of the carboxyl groups present in GO while the peak located at 1,615  $\text{cm}^{-1}$  might result from the skeletal vibration of the un-oxidized  $\text{sp}^2$  hybridized carbon in the graphitic structure [62,64]. The peak located at 1,400  $\text{cm}^{-1}$  corresponds to stretching vibration of the GO carboxyl group while the peak appearing at 1,220  $\text{cm}^{-1}$  typically results from the C–O–C stretching vibration. The other peaks appearing between 1,040 and 520  $\text{cm}^{-1}$  are associated with the C–O stretching of the GO epoxy groups [62,63]. The presence of respective functional groups as noted at the GO surface (Fig. 4) tend to initiate adsorption via bonding with the respective target adsorbate species and hence play a very important role in the overall removal of target aqueous pollutants.

The specific surface area, pore volume, and pore size attributes of synthesized GO were obtained using the

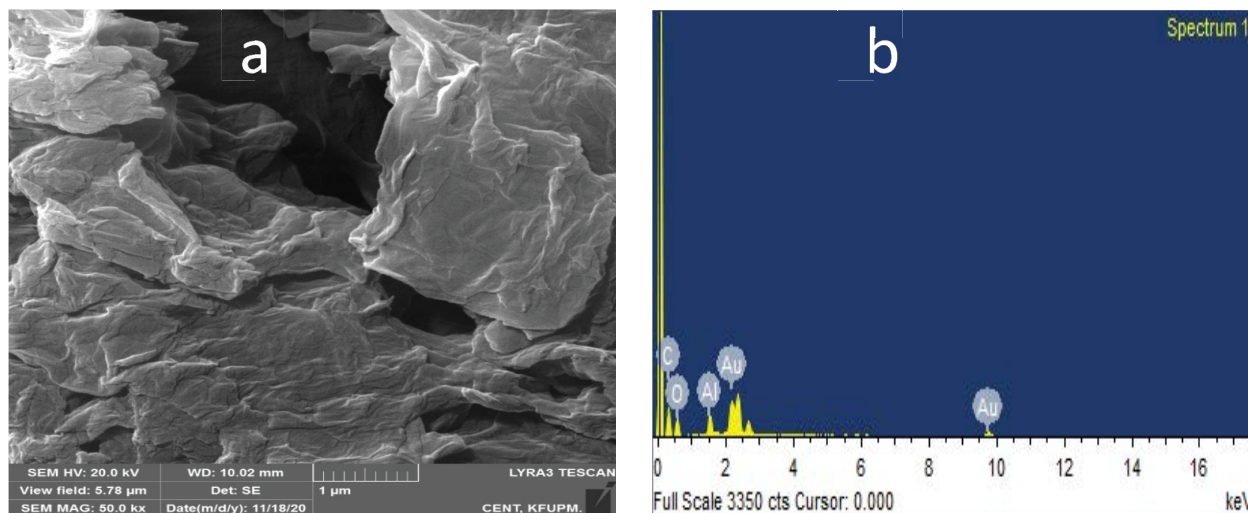


Fig. 3. (a) Morphological structure and (b) elemental composition of synthesized graphene oxide.

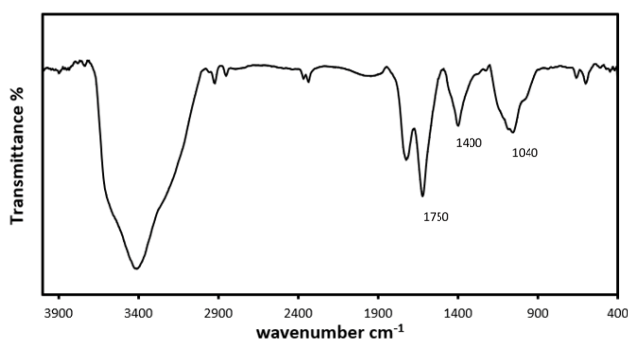


Fig. 4. FTIR spectra of synthesized graphene oxide (% transmittance as a function of inverse wavenumber).

$N_2$ -physisorption measurements conducted at 77 K. The respective  $N_2$  adsorption/desorption isotherm for GO as shown in Fig. 5 exhibits a type IV adsorption isotherm with hysteresis. The former is usually the characteristic of mesoporous structured adsorbents while the latter is usually observed for non-rigid aggregates having a wide pore size distribution and a slit-like shape [64], which is in line with the SEM image shown in Fig. 3a. The respective BET specific surface area, pore volume, and average pore size values are 92.0  $m^2/g$ , 0.295  $m^3/g$ , and 12.82 nm, respectively. As per the conventional classification of porous materials (i.e., microporous pore size <2 nm, mesoporous pore size 2–50 nm, macroporous pore size >50 nm) the produced GO fits into the mesoporous category [65].

### 3.2. Competitive removal of heavy metal species

After completing the surface characterization steps, the respective graphene oxide (GO) was also tested for the adsorption of cadmium, chromium, and lead species under varying mixed-competitive matrices. To that end, the effect of metals and GO-adsorbent onto metals adsorption capacity was investigated at three different metal-concentrations (i.e., 5, 7.5, and 10 mg/L) and three different GO-adsorbent

dosages (i.e., 0.2, 0.35, and 0.5 g/L). The RSM based central composite design (CCD) along with the respective four factors is given in Table 2, which also summarizes the overall removal of cadmium, chromium, and lead under respective competitive conditions. Table 2 also summarizes the removal of respective metal species for each competitive adsorption condition with chromium showing the highest adsorption followed by lead and cadmium. Furthermore, the respective GO dosage effects also typically indicate higher metal removal at higher GO dosages. The availability of higher surface adsorption sites at higher GO dosages yield higher metal removal from the aqueous phase. Nevertheless, the above-mentioned trend, that is, chromium > lead > cadmium, is also reflected in the respective GO dosage effect results. The detailed adsorption results for cadmium, chromium, and lead, along with the modeling optimization results, are provided below.

The competitive adsorption based cadmium removal results are shown in Fig. 6. The cadmium adsorption is noted to initially increase with the adsorbent dosage followed by a plateau (Fig. 6a).

The respective initial increase in cadmium adsorption is attributed to availability of increased adsorption sites, followed by a plateau indicative of saturation. On the other hand the overall cadmium adsorption capacity is generally reduced in the presence of both chromium and lead (Fig. 6c and d, respectively) that can be attributed to latter's competitive adsorption onto GO material. Furthermore, the RSM modeling results showed that cadmium removal is described best by a quadratic model Eq. (2):

$$\begin{aligned} \text{Adsorption capacity of cadmium} (1/\text{Sqrt}) = & 0.2488 \\ & - 0.084A + 0.0113B + 0.0401C \\ & + 0.0136D + 0.0675A^2 - 0.0444D^2 \end{aligned} \quad (2)$$

where  $A$ ,  $B$ ,  $C$ , and  $D$  terms represent the GO dosage, and concentrations of cadmium, chromium, and lead, respectively. The effect of the model terms was noted to be in the order  $A^2 > C > B > D$ . The predicted  $R^2$  and adjusted  $R^2$

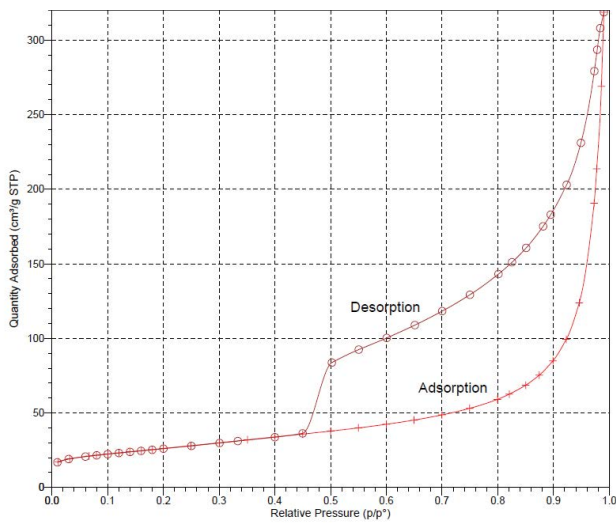


Fig. 5. N<sub>2</sub> adsorption–desorption isotherm of synthesized graphene oxide (N<sub>2</sub> adsorbed vs. relative pressure).

values are also noted to be in good agreement as given in Table 3. Furthermore, the RSM outcomes with  $p < 0.05$  typically imply significance whereas higher  $F$ -values indicate that the respective model terms have most significant effect on the response function [66–69]. To that end, the analysis of variance (ANOVA) analyses showed that the GO dosage and concentration of chromium and lead are significant model parameters with respective  $F$ -values of 195.12, 44.46, 5.10, and respective  $p$ -values of  $<0.0001$ ,  $<0.0001$ , and 0.0366 (Table 4). Furthermore, the normal distribution for normal probability vs. residuals plot (Fig. 7) and a linear fit between predicted and actual cadmium removal results (Fig. 8) support the respective RSM modeling outcomes.

The present work was further expanded to study the influence of GO dosage and also cadmium and lead concentration onto adsorption of chromium. Fig. 9a shows that as the adsorbent dosage was increased, the chromium adsorption capacity also increased with ~99% removal at 0.5 g/L of GO. Also (unlike the cadmium findings in Fig. 6) chromium removal shows minimum effect of both cadmium (Fig. 9b) and lead (Fig. 9d). Various functional groups and specifically

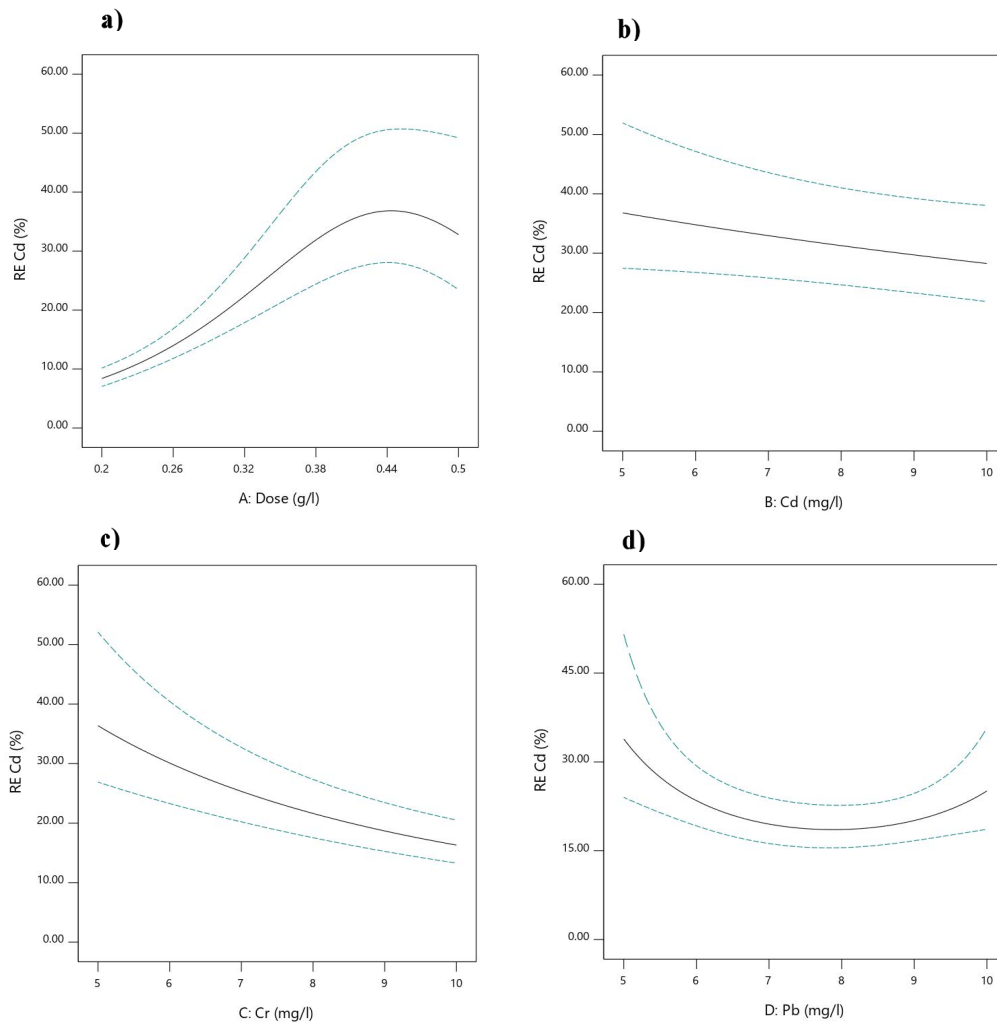


Fig. 6. Effect of (a) GO dosage, (b) cadmium concentration, (c) chromium concentration, and (d) lead concentration on to adsorption capacity of cadmium.

Table 3  
Fit statistics of quadratic model of cadmium adsorption capacity

Std. Dev.	0.0255	$R^2$	0.9377
Mean	0.2654	Adjusted $R^2$	0.9169
C.V. %	9.61	Predicted $R^2$	0.8674
		Adequate precision	22.0708

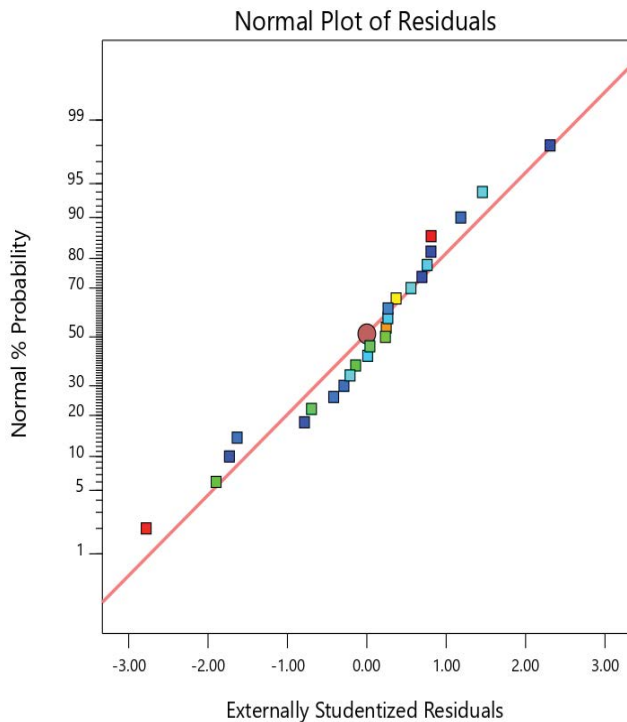


Fig. 7. Normal plot of residuals for cadmium adsorption capacity.

oxygen based functional groups were noted at the GO surface (Fig. 4). It is suggested that the electron rich oxygen surface functional species tend to initiate adsorption via bonding with the respective heavy metal species (Fig. 10).

Similar surface functional groups have been reported also for the magnetic graphene oxide for toxic metal species removal [44]. Also, the studied metals at pH 4 are dominantly having cationic speciation, which is also conducive for adsorption onto respective graphene oxide surface functional groups. Furthermore, the mesoporous nature of synthesized GO (as per Fig. 5 and discussion in section 3.1) is also conducive towards mass transfer of respective metal species within the adsorbent thus maximizing the utilization of available surface bonding sites. The chromium adsorption results were also modeled using the RSM approach and the respective best fit is given in Eq. (3):

$$\text{Adsorption capacity of chromium} = 82.61 + 9.78A - 0.3467B - 6.51C - 1.49D \quad (3)$$

where  $A$ ,  $B$ ,  $C$ , and  $D$  terms represent the GO dosage, and concentrations of cadmium, chromium, and lead, respectively. The predicted  $R^2$  is also in good agreement with the

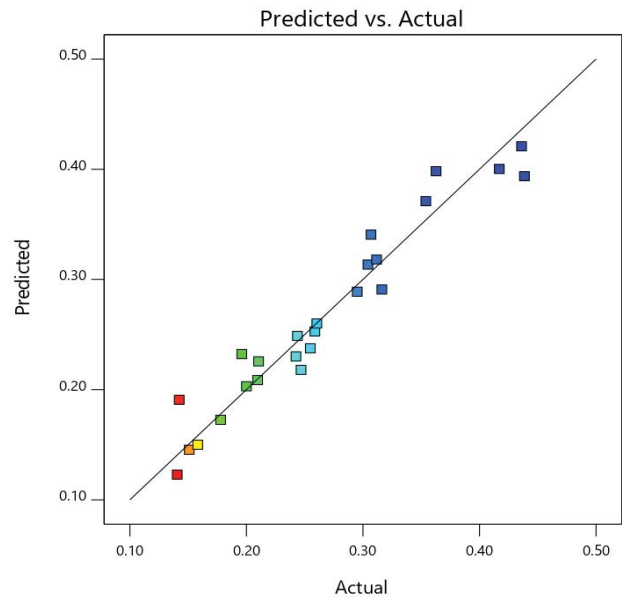


Fig. 8. Predicted vs. actual responses for cadmium adsorption capacity.

adjusted  $R^2$  (Table 5). Furthermore, the ANOVA findings in Table 6 indicate that the GO dosage and chromium concentration are significant parameters with respective  $F$ -values of 78.65 and 34.90, and  $p$ -values  $< 0.0001$ . Also, the respective normal probability plots (Fig. 11) and predicted vs. actual response plot (Fig. 12) show a good fit for the chromium RSM model. Also, for the adsorption kinetics, the respective experimental data was fitted to different kinetic models including zero-order, first-order, second-order and pseudo-second-order kinetic models. The best fit was noted for the pseudo-second-order kinetic model. Sheikhmohammadi et al. [46] who studied adsorption of chromium onto GO modified with 8-hydroxyquinoline also noted a similar kinetic trend. Similarly He et al. [15] also report a pseudo-second-order kinetic trend for functionalized GO application for chromium removal. A similar trend using GO has also been noted for cadmium adsorption [34].

After completing the adsorption of cadmium and chromium, the efficiency of synthesized GO material was also investigated under tertiary conditions for the competitive removal of lead. Fig. 13 that provides the respective results shows increasing lead removal with an increase in the GO dosage with upto 92% removal using 0.5 g/L of GO adsorbent.

Similarly Lingamdinne et al. [39] who studied lead adsorption using ferrite modified graphene oxide also report 99% lead removal using 0.55 g/L adsorbent dosage. Furthermore cadmium shows insignificant effect onto lead removal (Fig. 13b) and chromium shows some decrease (Fig. 13c). The RSM model fit yielded the following model equation [Eq. (4)]:

$$\begin{aligned} \text{Adsorption capacity of lead} = & 77.03 + 15.2A \\ & - 1.24B - 6.72C - 3.23D + 2.64AC \\ & - 2.25CD - 11.57A^2 + 5.24D^2 \end{aligned} \quad (4)$$

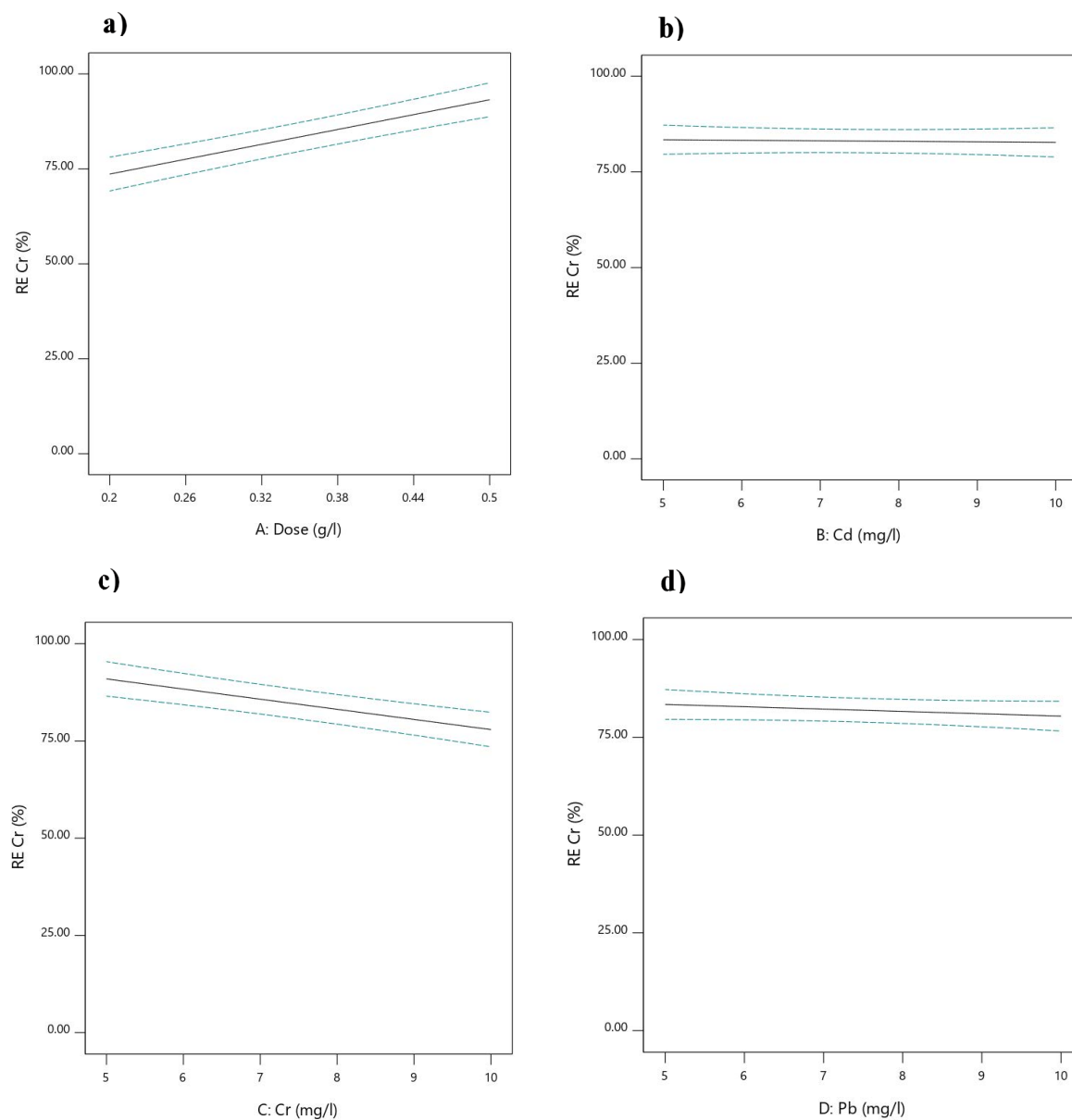


Fig. 9. Effect of (a) GO dosage, (b) cadmium concentration, (c) chromium concentration, and (d) lead concentration on to adsorption capacity of chromium.

Table 4  
ANOVA table of quadratic model of cadmium adsorption capacity

Source	Sum of squares	df	Mean square	F-value	p-value	Comment
Model	0.1762	6	0.0294	45.12	<0.0001	Significant
A-Dose	0.1270	1	0.1270	195.12	<0.0001	Significant
B-Cd	0.0023	1	0.0023	3.54	0.0763	
C-Cr	0.0289	1	0.0289	44.46	<0.0001	Significant
D-Pb	0.0033	1	0.0033	5.10	0.0366	Significant
A <sup>2</sup>	0.0146	1	0.0146	22.43	0.0002	Significant
D <sup>2</sup>	0.0063	1	0.0063	9.71	0.0060	Significant

where *A*, *B*, *C*, and *D* terms represent the GO dosage, and concentrations of cadmium, chromium, and lead, respectively. Also Table 7 shows that the adjusted  $R^2$  of 0.9386 is in reasonable agreement with the predicted  $R^2$  of 0.8959. Furthermore, Table 8 that provides the ANOVA findings indicates that the GO dosage and concentration of chromium and lead are significant parameters with respective *F*-values of 267.48, 52.27, and 12.09, and respective *p*-values of <0.0001, <0.0001, and 0.0031 as also reported earlier for RSM based process optimization modeling [50,70,71]. Furthermore, a comparison with some previous findings (Table 9) shows that the lead adsorption capacity is similar to the other GO studies [72–74]. It is suggested that the electron rich oxygen surface functional species at the GO surface (Fig. 4), tend to initiate adsorption via bonding with the respective heavy metal species. Also the normal probability plot (Fig. 14) and the lead removal predicted and actual responses (Fig. 15) also show a good fit.

These findings indicate that the respective RSM outcomes can be employed to model cadmium, chromium, and lead adsorption capacity using the synthesized GO-adsorbent under competitive tertiary conditions with a very reasonable

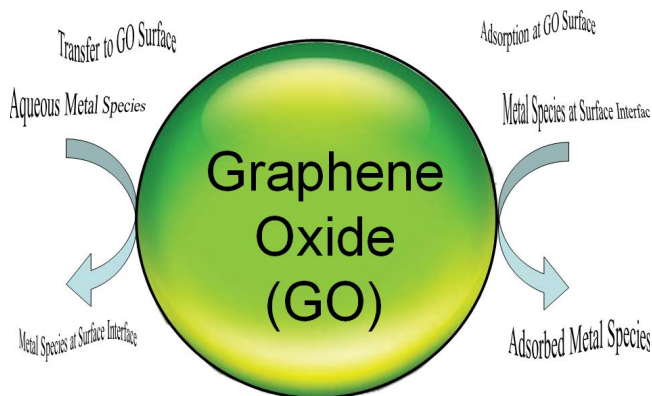


Fig. 10. A qualitative depiction of metal-species adsorption mechanism at the GO surface.

Table 5  
Fit statistics of linear model of chromium adsorption capacity

Std. Dev.	4.68	$R^2$	0.8524
Mean	82.61	Adjusted $R^2$	0.8229
C.V. %	5.66	Predicted $R^2$	0.7640
		Adequate precision	17.3360

Table 6  
ANOVA table of linear model of chromium adsorption capacity

Source	Sum of squares	df	Mean square	<i>F</i> -value	<i>p</i> -value	Comment
Model	2,527.52	4	631.88	28.87	<0.0001	Significant
<i>A</i> -Dose	1,721.27	1	1,721.27	78.65	<0.0001	Significant
<i>B</i> -Cd	2.16	1	2.16	0.0989	0.7565	–
<i>C</i> -Cr	763.87	1	763.87	34.90	<0.0001	Significant
<i>D</i> -Pb	40.21	1	40.21	1.84	0.1904	–

match between the experimental and model adsorption results. Furthermore, the synthesized GO shows a great potential to successfully remove both chromium and lead even under competitive tertiary conditions and hence has

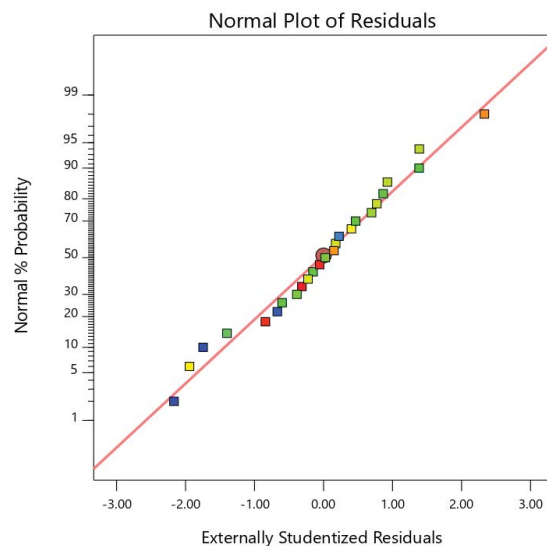


Fig. 11. Normal plot of residuals for chromium adsorption capacity.

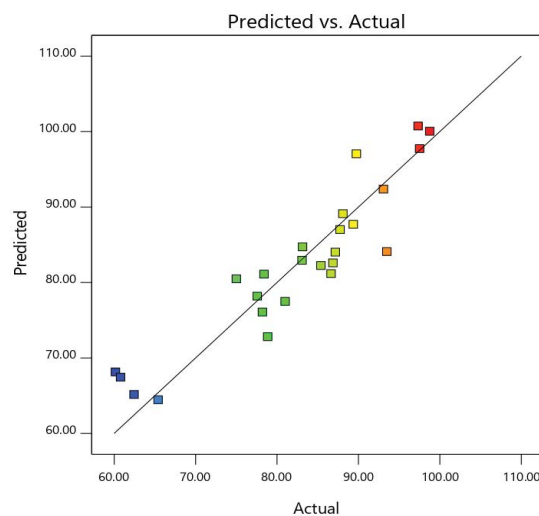


Fig. 12. Predicted vs. actual responses for chromium adsorption capacity.

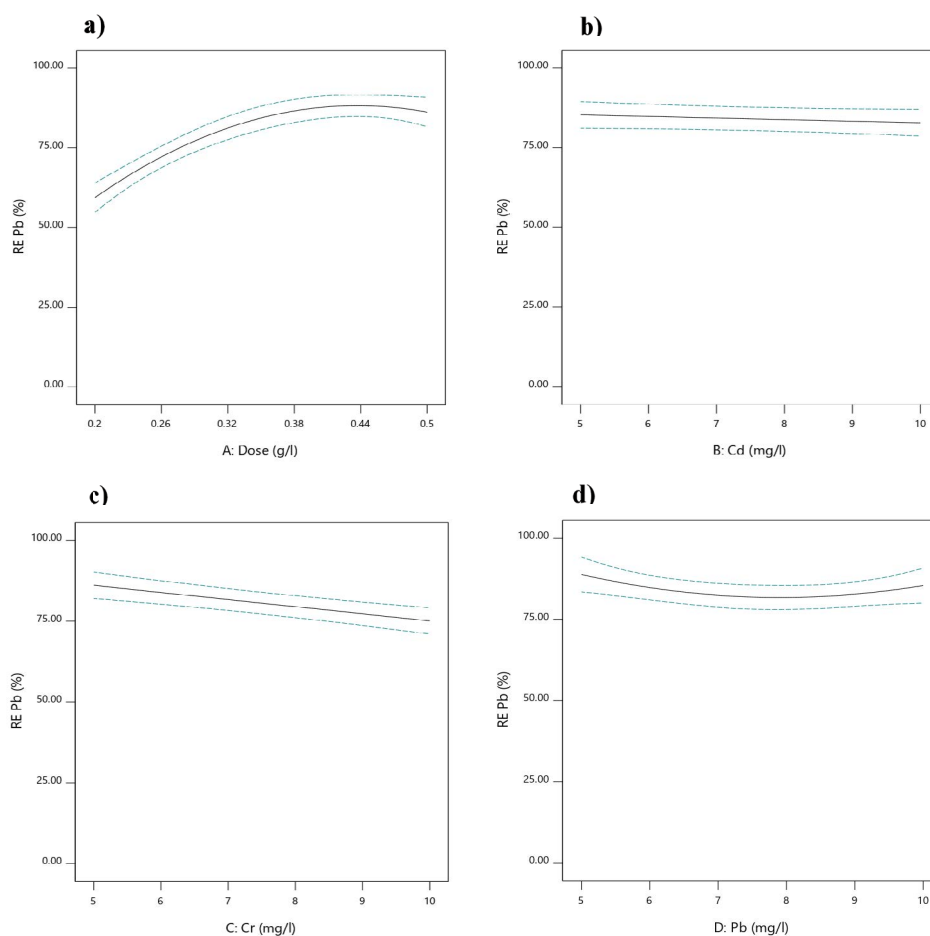


Fig. 13. Effect of (a) GO dosage, (b) cadmium concentration, (c) chromium concentration, and (d) lead concentration on to adsorption capacity of lead.

Table 7  
Fit statistics of quadratic model of lead adsorption capacity

Std. Dev.	3.94	$R^2$	0.9590
Mean	72.48	Adjusted $R^2$	0.9386
C.V. %	5.44	Predicted $R^2$	0.8959
		Adequate precision	22.3101

a great potential to be used for the treatment of respective wastewater streams.

#### 4. Conclusions

Results from the present study show that for tertiary cadmium, chromium and lead competitive adsorption onto mesoporous graphene oxide (GO), the removal of chromium from the tertiary mixture is almost complete (~99%). The removal of lead is also high at ~92%. However, the removal of cadmium is only about 51% that can be attributed to preferable competitive adsorption of chromium and lead. The FTIR results showed that the produced GO has several oxygen based functional groups important for the adsorption of target heavy metal species. Furthermore, the BET

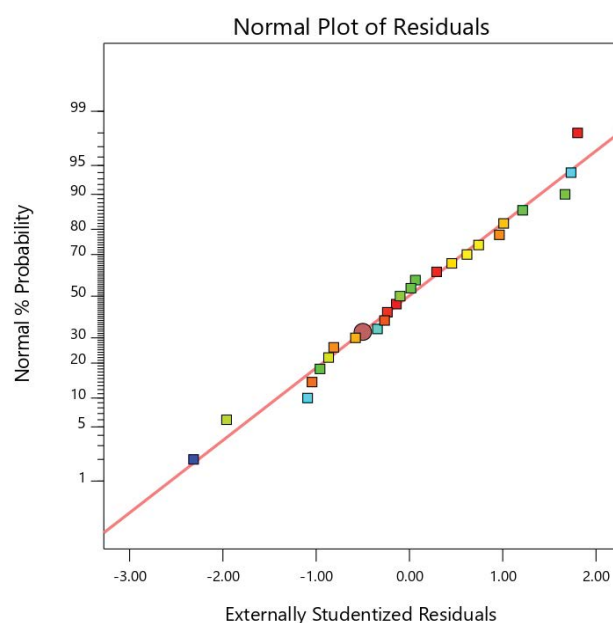


Fig. 14. Normal plot of residuals for lead adsorption capacity.

Table 8  
ANOVA table of quadratic model of lead adsorption capacity

Source	Sum of squares	df	Mean square	F-value	p-value	Comment
Model	5,825.09	8	728.14	46.82	<0.0001	Significant
A-Dose	4,159.73	1	4,159.73	267.48	<0.0001	Significant
B-Cd	27.71	1	27.71	1.78	0.2006	
C-Cr	812.87	1	812.87	52.27	<0.0001	Significant
D-Pb	187.99	1	187.99	12.09	0.0031	Significant
AC	111.49	1	111.49	7.17	0.0165	Significant
CD	81.28	1	81.28	5.23	0.0362	Significant
A <sup>2</sup>	428.92	1	428.92	27.58	<0.0001	Significant
D <sup>2</sup>	88.20	1	88.20	5.67	0.0300	

Table 9  
Comparison with some previous GO studies for metals removal

Adsorbent	Contaminant	Conc. (ppm)	Dose (g/L)	pH	RE (%)	References
GO	Pb(II), Cd(II)	1	0.1	2–8	>99%, >90%	[28]
GO	Cd(II)	10	0.5	4	96.72%	[72]
MDFGO	Pb(II), Cd(II)	50	0.033	6.2	99.6%, 99.4%	[73]
GO-OM	Pb(II), Cd(II)	5	1	9	99%, 95%	[74]
GO	Pb(II), Cd(II), Cr(III)	5, 7.5, 10	0.5	4	92%, 51%, and 99%	Present study

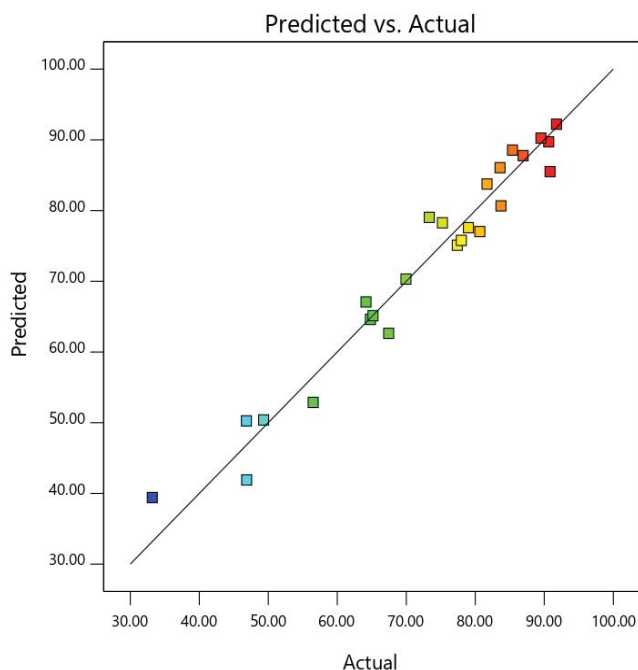


Fig. 15. Predicted vs. actual responses for lead adsorption capacity.

characterization results indicated that the synthesized GO is mesoporous that is also supportive of an enhanced mass transfer to the surface bonding sites. The RSM based modeling and optimization outcomes also supported a very good fit to the experimental results. For lead removal, the

respective ANOVA findings showed that the GO dosage and concentration of lead and chromium are the significant model parameters with respective *F*-values of 267.48, 52.27, and 12.09, and *p*-values of <0.0001, <0.0001, and 0.0031. The low *p*-values do support a good model fit. Similar trends were also noted for chromium and cadmium adsorption RSM modeling and optimization.

#### Acknowledgments

The authors are thankful to the Civil and Environmental Department and Chemical Engineering Department at the King Fahd University of Petroleum and Minerals (KFUPM) for providing the lab facilities. This work was also partially supported by the Deanship of Scientific Research (DSR) at King Fahd University of Petroleum and Minerals (KFUPM) through Internal Research Grant # DF191022.

#### References

- [1] O. Faroon, N. Roney, J. Taylor, A. Ashizawa, M.H. Lumpkin, D.J. Plewak, Acrolein environmental levels and potential for human exposure, *Toxicol. Ind. Health*, 24 (2008) 543–564.
- [2] J. Namieśnik, A. Rabajczyk, The speciation and physico-chemical forms of metals in surface waters and sediments, *Chem. Speciation Bioavailability*, 22 (2010) 1–24.
- [3] J.Y. Lim, N.M. Mubarak, E.C. Abdullah, S. Nizamuddin, M. Khalid, Inamuddin, Recent trends in the synthesis of graphene and graphene oxide based nanomaterials for removal of heavy metals – a review, *J. Ind. Eng. Chem.*, 66 (2018) 29–44.
- [4] G. Bhanjana, N. Dilbaghi, K.-H. Kim, S. Kumar, Carbon nanotubes as sorbent material for removal of cadmium, *J. Mol. Liq.*, 242 (2017) 966–970.
- [5] J. Acharya, U. Kumar, B.C. Meikap, Thermodynamic characterization of adsorption of lead(II) ions on activated

- carbon developed from tamarind wood from aqueous solution, *S. Afr. J. Chem. Eng.*, 18 (2013) 70–76.
- [6] M.K. Mondal, Removal of Pb(II) ions from aqueous solution using activated tea waste: adsorption on a fixed-bed column, *J. Environ. Manage.*, 90 (2009) 3266–3271.
- [7] S. Yang, J. Hu, C. Chen, D. Shao, X. Wang, Mutual effects of Pb(II) and humic acid adsorption on multiwalled carbon nanotubes/polyacrylamide composites from aqueous solutions, *Environ. Sci. Technol.*, 45 (2011) 3621–3627.
- [8] M. Mom, M. Purenovi, A. Boji, A. Zarubica, M. Ran, Removal of lead(II) ions from aqueous solutions by adsorption onto pine cone activated carbon, *Desalination*, 276 (2011) 53–59.
- [9] S. Huang, S. Song, R. Zhang, T. Wen, X. Wang, S. Yu, W. Song, T. Hayat, A. Alsaedi, X. Wang, Construction of layered double hydroxides/hollow carbon microsphere composites and its applications for mutual removal of Pb(II) and humic acid from aqueous solutions, *ACS Sustainable Chem. Eng.*, 5 (2017) 11268–11279.
- [10] B. Singha, S.K. Das, Removal of Pb(II) ions from aqueous solution and industrial effluent using natural biosorbents, *Environ. Sci. Pollut. Res.*, 19 (2012) 2212–2226.
- [11] M. Arbabi, M., Hemati, S., Amiri, Removal of lead ions from industrial wastewater: a review of removal methods, *Int. J. Epidemiol. Res.*, 2 (2015) 105–109.
- [12] M. Özacar, İ. Ayhan Şengil, H. Türkmenler, Equilibrium and kinetic data, and adsorption mechanism for adsorption of lead onto valonia tannin resin, *Chem. Eng. J.*, 143 (2008) 32–42.
- [13] J. Namieśnik, A.R. Jczyk, Speciation analysis of chromium in environmental samples, *Environ. Sci. Technol.*, 3389 (2012) 327–377.
- [14] J. Wang, P. Wang, H. Wang, J. Dong, W. Chen, X. Wang, S. Wang, T. Hayat, A. Alsaedi, X. Wang, Preparation of molybdenum disulfide coated Mg/Al layered double hydroxide composites for efficient removal of chromium(VI), *ACS Sustainable Chem. Eng.*, 5 (2017) 7165–7174.
- [15] C. He, Z. Yang, J. Ding, Y. Chen, X. Tong, Y. Li, Effective removal of Cr(VI) from aqueous solution by 3-aminopropyltriethoxysilane-functionalized graphene oxide, *Colloids Surf., A*, 520 (2017) 448–458.
- [16] F. Teshale, R. Karthikeyan, O. Sahu, Synthesized bioadsorbent from fish scale for chromium(III) removal, *Micron*, 130 (2020) 102817, doi: 10.1016/j.micron.2019.102817.
- [17] T. Saheed Kazeem, Treatment of aqueous selenocyanate anions using electrocoagulation, *Int. J. Electrochem. Sci.*, 14 (2019) 10538–10564.
- [18] M.S. Vohra, Selenocyanate (SeCN<sup>-</sup>) contaminated wastewater treatment using TiO<sub>2</sub> photocatalysis: SeCN<sup>-</sup> complex destruction, intermediates formation, and removal of selenium species, *Fresenius Environ. Bull.*, 24 (2015) 1108–1118.
- [19] B.A. Labaran, M.S. Vohra, Photocatalytic removal of selenite and selenate species: effect of EDTA and other process variables, *Environ. Technol. (United Kingdom)*, 35 (2014) 1091–1100.
- [20] B.A. Labaran, M.S. Vohra, Competitive adsorption of selenite [Se(IV)], selenate [Se(VI)] and selenocyanate [SeCN<sup>-</sup>] species onto TiO<sub>2</sub>: Experimental findings and surface complexation modelling, *Desal. Water Treat.*, 124 (2018) 267–278.
- [21] T. Mohammed, T.S. Kazeem, M.H. Essa, B.A. Labaran, M.S. Vohra, Comparative study on electrochemical treatment of arsenite: effects of process parameters, sludge characterization and kinetics, *Arabian J. Sci. Eng.*, 45 (2020) 3799–3815.
- [22] M.S. Vohra, M.S. Al-Suwaiyan, M.H. Essa, M.M.I. Chowdhury, M.M. Rahman, B.A. Labaran, Application of solar photocatalysis and solar photo-Fenton processes for the removal of some critical charged pollutants: mineralization trends and formation of reaction intermediates, *Arabian J. Sci. Eng.*, 41 (2016) 3877–3887.
- [23] M.J. Allen, V.C. Tung, R.B. Kaner, Honeycomb carbon: a review of graphene, *Chem. Rev.*, 110 (2010) 132–145.
- [24] A. Lerf, H. He, M. Förster, J. Klinowski, Structure of graphite oxide revisited, *J. Phys. Chem. B*, 102 (1998) 4477–4482.
- [25] G. Zhao, J. Li, X. Ren, C. Chen, X. Wang, Few-layered graphene oxide nanosheets as superior sorbents for heavy metal ion pollution management, *Environ. Sci. Technol.*, 45 (2011) 10454–10462.
- [26] L.P. Lingamdinne, Y.L. Choi, I.S. Kim, J.K. Yang, J.R. Koduru, Y.Y. Chang, Preparation and characterization of porous reduced graphene oxide based inverse spinel nickel ferrite nanocomposite for adsorption removal of radionuclides, *J. Hazard. Mater.*, 326 (2017) 145–156.
- [27] L.P. Lingamdinne, J.R. Koduru, R.R. Karri, A comprehensive review of applications of magnetic graphene oxide based nanocomposites for sustainable water purification, *J. Environ. Manage.*, 231 (2019) 622–634.
- [28] R. Sitko, E. Turek, B. Zawisza, E. Malicka, E. Talik, J. Heimann, A. Gagor, B. Feist, R. Wrzalik, Adsorption of divalent metal ions from aqueous solutions using graphene oxide, *Dalton Trans.*, 42 (2013) 5682–5689.
- [29] C. Hontoria-Lucas, A.J. López-Peinado, J. de D. López-González, M.L. Rojas-Cervantes, R.M. Martín-Aranda, Study of oxygen-containing groups in a series of graphite oxides: physical and chemical characterization, *Carbon N. Y.*, 33 (1995) 1585–1592.
- [30] R. Sitko, B. Zawisza, E. Malicka, Modification of carbon nanotubes for preconcentration, separation and determination of trace-metal ions, *TrAC, Trends Anal. Chem.*, 37 (2012) 22–31.
- [31] S. Kaushal, N. Kaur, M. Kaur, P.P. Singh, Dual-responsive pectin/graphene oxide (Pc/GO) nano-composite as an efficient adsorbent for Cr(III) ions and photocatalyst for degradation of organic dyes in waste water, *J. Photochem. Photobiol., A*, 403 (2020) 112841, doi: 10.1016/j.jphotochem.2020.112841.
- [32] A.O. Salawudeen, B.S. Tawabini, A.M. Al-shaibani, A. Saleh, Poly(2-hydroxyethyl methacrylate) grafted graphene oxide for cadmium removal from water with interaction mechanisms, *Environ. Nanotechnol. Monit. Manage.*, 13 (2020) 100288, doi: 10.1016/j.enmm.2020.100288.
- [33] S.Z.N. Ahmad, W.N.W. Salleh, N.H. Ismail, N. Rosman, N.A.M. Razali, R. Hamdan, A.F. Ismail, Zeolitic imidazolate framework-L incorporated graphene oxide hybrid for cadmium removal, *Mater. Today: Proc.*, 42 (2021) 8–14.
- [34] Y. Zhang, W. Peng, L. Xia, S. Song, Adsorption of Cd(II) at the interface of water and graphene oxide prepared from flaky graphite and amorphous graphite, *J. Environ. Chem. Eng.*, 5 (2017) 4157–4164.
- [35] K.C. Lai, L.Y. Lee, B.Y.Z. Hiew, S. Thangalazhy-Gopakumar, S. Gan, Facile synthesis of xanthan biopolymer integrated 3D hierarchical graphene oxide/titanium dioxide composite for adsorptive lead removal in wastewater, *Bioresour. Technol.*, 309 (2020) 123296, doi: 10.1016/j.biortech.2020.123296.
- [36] Y. Chen, W. Jiang, C. Zhao, Z. Liu, Y. Liang, Facile modification of graphene oxide by humic acid for enhancing hexavalent chromium photoreduction, *J. Environ. Chem. Eng.*, 9 (2021) 104759, doi: 10.1016/j.jece.2020.104759.
- [37] J.H. Lee, J.-A. Park, H.-G. Kim, J.-H. Lee, S.-H. Cho, K. Choi, K.-W. Jung, S.-Y. Lee, J.-W. Choi, Most suitable amino silane molecules for surface functionalization of graphene oxide toward hexavalent chromium adsorption, *Chemosphere*, 251 (2020) 126387, doi: 10.1016/j.chemosphere.2020.126387.
- [38] P.L. Narayana, L.P. Lingamdinne, R.R. Karri, S. Devanesan, M.S. AlSalhi, N.S. Reddy, Y.-Y. Chang, J. Reddy Koduru, Predictive capability evaluation and optimization of Pb(II) removal by reduced graphene oxide-based inverse spinel nickel ferrite nanocomposite, *Environ. Res.*, 204 (2022) 112029, doi: 10.1016/j.envres.2021.112029.
- [39] L.P. Lingamdinne, J.R. Koduru, Y.Y. Chang, R.R. Karri, Process optimization and adsorption modeling of Pb(II) on nickel ferrite-reduced graphene oxide nano-composite, *J. Mol. Liq.*, 250 (2018) 202–211.
- [40] M. Li, Q. Hu, H. Shan, W. Yu, Z.-X. Xu, Fabrication of copper phthalocyanine/reduced graphene oxide nanocomposites for efficient photocatalytic reduction of hexavalent chromium, *Chemosphere*, 263 (2021) 128250, doi: 10.1016/j.chemosphere.2020.128250.
- [41] X. Li, H. Zhou, W. Wu, S. Wei, Y. Xu, Y. Kuang, Studies of heavy metal ion adsorption on chitosan/sulfdryl-functionalized graphene oxide composites, *J. Colloid Interface Sci.*, 448 (2015) 389–397.

- [42] C. Bai, L. Wang, Z. Zhu, Adsorption of Cr(III) and Pb(II) by graphene oxide/alginate hydrogel membrane: characterization, adsorption kinetics, isotherm and thermodynamics studies, *Int. J. Biol. Macromol.*, 147 (2020) 898–910.
- [43] M.E. Mahmoud, M.M. Osman, H. Abdel-Aal, G.M. Nabil, Microwave-assisted adsorption of Cr(VI), Cd(II) and Pb(II) in presence of magnetic graphene oxide-covalently functionalized-tryptophan nanocomposite, *J. Alloys Compd.*, 823 (2020) 153855, doi: 10.1016/j.jallcom.2020.153855.
- [44] A. Sheikhmohammadi, S.M. Mohseni, B. Hashemzadeh, E. Asgari, R. Sharafkhani, M. Sardar, M. Sarkhosh, M. Almasiane, Fabrication of magnetic graphene oxide nanocomposites functionalized with a novel chelating ligand for the removal of Cr(VI): modeling, optimization, and adsorption studies, *Desal. Water Treat.*, 160 (2019) 297–307.
- [45] A. Sheikhmohammadi, B. Hashemzadeh, A. Alinejad, S.M. Mohseni, M. Sardar, R. Sharafkhani, M. Sarkhosh, E. Asgari, A. Bay, Application of graphene oxide modified with the phenopyridine and 2-mercaptobenzothiazole for the adsorption of Cr(VI) from wastewater: optimization, kinetic, thermodynamic and equilibrium studies, *J. Mol. Liq.*, 285 (2019) 586–597.
- [46] A. Sheikhmohammadi, S.M. Mohseni, R. Khodadadi, M. Sardar, M. Abtahi, S. Mahdavi, H. Keramati, Z. Dahaghin, S. Rezaei, M. Almasian, M. Sarkhosh, M. Faraji, S. Nazari, Application of graphene oxide modified with 8-hydroxyquinoline for the adsorption of Cr(VI) from wastewater: optimization, kinetic, thermodynamic and equilibrium studies, *J. Mol. Liq.*, 233 (2017) 75–88.
- [47] Y. Zhang, S. Zhang, T.S. Chung, Nanometric graphene oxide framework membranes with enhanced heavy metal removal via nanofiltration, *Environ. Sci. Technol.*, 49 (2015) 10235–10242.
- [48] Y. Zhang, S. Zhang, J. Gao, T.S. Chung, Layer-by-layer construction of graphene oxide (GO) framework composite membranes for highly efficient heavy metal removal, *J. Membr. Sci.*, 515 (2016) 230–237.
- [49] H. Rasoulzadeh, A. Sheikhmohammadi, M. Abtahi, M. Alipour, B. Roshan, Predicting the capability of diatomite magnano composite boosted with polymer extracted from brown seaweeds for the adsorption of cyanide from water solutions using the response surface methodology: modelling and optimisation, *Int. J. Environ. Anal. Chem.*, (2021) 1–14, doi: 10.1080/03067319.2021.1931160.
- [50] E. Asgari, A. Sheikhmohammadi, J. Yeganeh, Application of the Fe<sub>3</sub>O<sub>4</sub>-chitosan nano-adsorbent for the adsorption of metronidazole from wastewater: optimization, kinetic, thermodynamic and equilibrium studies, *Int. J. Biol. Macromol.*, 164 (2020) 694–706.
- [51] D.C. Marcano, D.V. Kosynkin, J.M. Berlin, A. Sinitskii, Z. Sun, A. Slesarev, L.B. Alemany, W. Lu, J.M. Tour, Improved synthesis of graphene oxide, *ACS Nano*, 4 (2010) 4806–4814.
- [52] S.S. Ranade, P. Thiagarajan, Selection of a design for response surface, *IOP Conf. Ser.: Mater. Sci. Eng.*, 263 (2017) 022043.
- [53] Q. Huang, H.J. Sun, T.J. Peng, The influence of temperature and oxidation time on the preparation of graphite oxide, *Adv. Mater. Res.*, 366 (2011) 291–295.
- [54] X.-j. Hu, Y.-g. Liu, H. Wang, A.-w. Chen, G.-m. Zeng, S.-m. Liu, Y.-m. Guo, X. Hu, T.-t. Li, Y.-q. Wang, L. Zhou, S.-h. Liu, Removal of Cu(II) ions from aqueous solution using sulfonated magnetic graphene oxide composite, *Sep. Purif. Technol.*, 108 (2013) 189–195.
- [55] P. Liu, Y. Huang, L. Wang, A facile synthesis of reduced graphene oxide with Zn powder under acidic condition, *Mater. Lett.*, 91 (2013) 125–128.
- [56] L. Stobinski, B. Lesiak, A. Malolepszy, M. Mazurkiewicz, B. Mierzwa, J. Zemek, P. Jiricek, I. Bieloshapka, Graphene oxide and reduced graphene oxide studied by the XRD, TEM and electron spectroscopy methods, *J. Electron. Spectrosc. Relat. Phenom.*, 195 (2014) 145–154.
- [57] S.-M. Hong, S.H. Kim, K.B. Lee, Adsorption of carbon dioxide on 3-aminopropyl-triethoxysilane modified graphite oxide, *Energy Fuels*, 27 (2013) 3358–3363.
- [58] M.P. Araújo, O.S.G.P. Soares, A.J.S. Fernandes, M.F.R. Pereira, C. Freire, Tuning the surface chemistry of graphene flakes: new strategies for selective oxidation, *RSC Adv.*, 7 (2017) 14290–14301.
- [59] J. Pokhrel, N. Bhoria, S. Anastasiou, T. Tsoufis, D. Gournis, G. Romanos, G.N. Karanikolos, CO<sub>2</sub> adsorption behavior of amine-functionalized ZIF-8, graphene oxide, and ZIF-8/graphene oxide composites under dry and wet conditions, *Microporous Mesoporous Mater.*, 267 (2018) 53–67.
- [60] X. Xie, Y. Zhou, K. Huang, Advances in microwave-assisted production of reduced graphene oxide, *Front. Chem.*, 7 (2019) 1–11.
- [61] F. Pendolino, N. Armata, Synthesis, Characterization and Models of Graphene Oxide, F. Pendolino, N. Armata, Eds., *Graphene Oxide in Environmental Remediation Process*, SpringerBriefs in Applied Sciences and Technology, Springer, Cham, 2017, pp. 5–21.
- [62] Rattana, S. Chaivakun, N. Witit-anun, N. Nuntawong, P. Chindaudom, S. Oaew, C. Kedkeaw, P. Limsuwan, Preparation and characterization of graphene oxide nanosheets, *Procedia Eng.*, 32 (2012) 759–764.
- [63] X. Mei, J. Ouyang, Ultrasonication-assisted ultrafast reduction of graphene oxide by zinc powder at room temperature, *Carbon N. Y.*, 49 (2011) 5389–5397.
- [64] A.M. Alkadhém, M.A.A. Elgzoly, S.A. Onaizi, Novel amine-functionalized magnesium oxide adsorbents for CO<sub>2</sub> capture at ambient conditions, *J. Environ. Chem. Eng.*, 8 (2020) 103968, doi: 10.1016/j.jece.2020.103968.
- [65] K.S.W. Sing, D.H. Everett, R.A.W. Haul, L. Moscou, R.A. Pierotti, J. Rouquerol, T. Siemieniewska, Reporting physisorption data for gas/solid systems with special reference to the determination of surface area and porosity, *Pure Appl. Chem.*, 57 (1985) 603–619.
- [66] B.A. Labaran, M.S. Vohra, Application of activated carbon produced from phosphoric acid-based chemical activation of oil fly ash for the removal of some charged aqueous phase dyes: role of surface charge, adsorption kinetics, and modeling, *Desal. Water Treat.*, 57 (2016) 16034–16052.
- [67] B.A. Labaran, M.S. Vohra, Solar photocatalytic removal of selenite, selenate, and selenocyanate species, *CLEAN – Soil, Air, Water*, 45 (2017) 1600268, doi: 10.1002/cle.201600268.
- [68] M.S. Vohra, Photocatalytic treatment of mixed selenocyanate and phenol streams: process modeling, optimization, and kinetics, *Environ. Prog. Sustainable Energy*, 13401 (2020) 1–11.
- [69] S.A.A. Ahmed, M.S. Vohra, Treatment of aqueous selenocyanate (SeCN<sup>-</sup>) using combined TiO<sub>2</sub> photocatalysis and 2-line ferrihydrite adsorption, *Desal. Water Treat.*, 211 (2021) 267–279.
- [70] H. Rasoulzadeh, A. Sheikhmohammadi, E. Asgari, B. Hashemzadeh, The adsorption behaviour of triclosan onto magnetic bio polymer beads impregnated with diatomite, *Int. J. Environ. Anal. Chem.*, (2021) 1–13, doi: 10.1080/03067319.2021.1922684.
- [71] E. Asgari, F. Mohammadi, H. Nourmoradi, A. Sheikhmohammadi, Z. Rostamifasih, B. Hashemzadeh, H. Arfaeinia, Heterogeneous catalytic degradation of nonylphenol using persulphate activated by natural pyrite: response surface methodology modelling and optimisation, *Int. J. Environ. Anal. Chem.*, (2020) 1–20, doi: 10.1080/03067319.2020.1807528.
- [72] X. Xue, J. Xu, S.A. Baig, X. Xu, Synthesis of graphene oxide nanosheets for the removal of Cd(II) ions from acidic aqueous solutions, *J. Taiwan Inst. Chem. Eng.*, 59 (2016) 365–372.
- [73] M. Ghorbani, A. Shams, O. Seyedin, N. Afshar Lahoori, Magnetic ethylene diamine-functionalized graphene oxide as novel sorbent for removal of lead and cadmium ions from wastewater samples, *Environ. Sci. Pollut. Res.*, 25 (2018) 5655–5667.
- [74] J. Wei, M.F. Aly Aboud, I. Shakir, Z. Tong, Y. Xu, Graphene oxide-supported organo-montmorillonite composites for the removal of Pb(II), Cd(II), and As(V) contaminants from water, *ACS Appl. Nano Mater.*, 3 (2020) 806–813.